# Protist-Facilitated Particle Transport Using Emulated Soil Micromodels

Rebecca L. Rubinstein,[†] Andrea L. Kadilak,[‡] Virginia C. Cousens,[‡] Daniel J. Gage,[§] and Leslie M. Shor[*,‡,‖]

[†]Department of Civil and Environmental Engineering, [‡]Department of Chemical and Biomolecular Engineering, [§]Department of Molecular and Cellular Biology, and [‖]Center for Environmental Sciences and Engineering, University of Connecticut, Storrs, Connecticut 06269, United States

Ⓢ Supporting Information

**ABSTRACT:** Microbial processes in the subsurface can be visualized directly using micromodels to emulate pore-scale geometries. Here, emulated soil micromodels were used to measure transport of fluorescent beads in the presence and absence of the soil ciliate *Colpoda* sp. under quiescent conditions. Beads alone or beads with protists were delivered to the input wells of replicate micromodels that contained three 20 mm² channels emulating a sandy loam microstructure. Bead abundance in microstructured channels was measured by direct counts of tiled confocal micrographs. For channels with protists, average bead abundances were approximately 320, 560, 710, 830, and 790 mm$^{-2}$ after 1, 2, 3, 5, and 10 days, respectively, versus 0, 0, 0.3, 7.8, and 45 mm$^{-2}$ without protists. Spatial and temporal patterns of bead abundance indicate that protist-facilitated transport is not a diffusive-type process but rather a function of more complex protist behaviors, including particle uptake and egestion and motility in a microstructured habitat. Protist-facilitated transport may enhance particle mixing in the soil subsurface and could someday be used for targeted delivery of nanoparticles, encapsulated chemicals, or bacteria for remediation and agriculture applications.
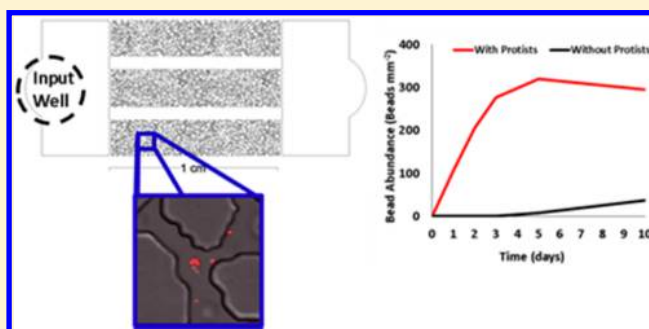
## INTRODUCTION

In recent years, there has been a growing appreciation for the importance of protists in mediating subsurface soil microbial processes, including contaminant uptake, terrestrial system productivity, and bioremediation. Protists are abundant in surface soils and in the deeper subsurface. For example, Kinner et al. measured populations of nanoflagellates exceeding 10⁴ protists per gram dry weight in an organically contaminated sandy aquifer.[1] Protist populations can respond to changes in bacterial populations under biostimulation conditions and induce a secondary turnover of biomass carbon.[2] Interactions of bacteria and protist populations during biostimulation have important implications for biodegradation and reactive transport modeling. Apart from the typical predator–prey relationship, protists may act as a vector to enhance transport of bacteria or other microparticles through soil.

The effects of protists on contaminant degradation are mixed; some reports have shown benefits, while others have shown inhibition. For example, Tso and Taghon found enhanced naphthalene degradation by up to a factor of 4 in the presence of grazing protists compared to grazing-inhibited controls, perhaps because of a selective grazing mechanism.[3] Alternatively, Cunningham et al. found trichloroethene (TCE) degradation was inhibited by grazing in fractured bedrock microcosms.[4] Theoretical work that sought to directly evaluate the impact of predator–prey interactions on the biodegradation of naphthalene found instances of enhanced biodegradation,[5] but this work did not account for the effects of the soil physical microstructures. The physical microstructures in a microbial habitat are known to constrain microbial spatial distributions, with most soil bacteria found in pores between 0.8 and 9 $\mu$m in diameter,[6] likely because of size exclusion of their natural predators, the soil protists. Bacteria and protists alike are limited to hydraulically connected regions of soil, and habitat discontinuity in unsaturated regions is believed to promote bacterial community diversity in unsaturated soils.[7]

Often, the lack of mixing in the subsurface can limit the rate and extent of *in situ* biodegradation.[8] Various studies have sought an improved means of delivering the bacteria responsible for remediation directly to the site of contamination. Wick et al. evaluated electrokinetic transport of polycyclic aromatic hydrocarbon (PAH)-degrading bacteria in a model aquifer and found bacteria only moved in the presence of a direct current, although the extent of movement, impact on degradation rates, and viability after prolonged exposure were strain-dependent.[9] Kohlmeier et al. considered fungal hyphae as potential pathways for dispersal of PAH-degrading bacteria and

found that efficacy was highly dependent upon the specific organisms used, but for some combinations, bacterial dispersal was enhanced.[10] Finally, Singer et al. investigated earthworms as a vector for transport of polychlorinated biphenyl-degrading bacteria and found that, while degradation rates varied by soil treatment, bacterial infiltration rates were improved in the presence of earthworms and that this effect increased with depth.[11]

Motile bacteria can move independently through porous media, but they are hampered by relatively slow swimming speeds and the predominance of the biofilm morphology. Free-living (planktonic) bacteria can swim on the order of 20 $\mu$m/s in short run lengths;[12] they can chemotact toward attractants and can be flushed through porous media with percolating water.[13] In the subsurface, however, the majority of bacteria are present in biofilms,[7] which are essentially immobile. The presence of attached bacteria has been linked to slower movement of soil ciliates through columns filled with porous media, suggesting active grazing, which may also lead to remobilization of bacteria from biofilms.[14] In soil microcosms, two common soil bacteria, *Rhizobium japonicum* and *Pseudomonas putida*, were found not to move below 2.7 cm soil depth without a vector when the top 2.4 cm was inoculated.[13] The maximum spreading rate of surface-attached biocontrol *Pseudomonas fluorescens* strains is just a few micrometers per hour,[15] about 5 orders of magnitude slower than ciliates, which swim for short runs at up to 400 $\mu$m/s.[16] After bacteria are ingested by protists, digestion rates are species-specific and affected by the overall availability of food to the protists,[17] but viable bacteria may be secreted in food vacuoles. Recently, First et al.[18] demonstrated viable *Campylobacter jejuni* are egested from the soil ciliate *Colpoda*. Additionally, Brock et al. showed that the social amoeba, *Dictyostelium discoideum*, carry bacteria to new habitats via spore dispersal.[19]

The goal of this study was to determine if protists can facilitate transport of bacteria-sized particles in a physically complex microstructure. Protist-facilitated transport in soil may enhance important ecosystem services provided by bacteria, which encompass both remediation and agriculture. Physical microstructure and microbial community function are strongly interrelated,[20] and conserving a realistic physical microstructure is particularly important in evaluating pore-scale transport processes. Microfluidics have been increasingly used to directly observe microscale processes, including bacterial chemotaxis,[21] protist mobility,[22] bacterial colony organization,[23] and the stability of multispecies communities.[24] Here, microfluidic devices were developed to emulate the microstructure of a sandy loam and were used to directly visualize protist-facilitated transport at the pore scale. Ultimately, a better understanding of the system function in the subsurface could lead to improved predictions of biogeochemical processes and enhanced environmental biotechnology for remediating contamination and improving agriculture.

## ■ MATERIALS AND METHODS

**Biological Cultures and Procedures.** *Protists. Colpoda* sp. are naturally occurring soil ciliates that form cysts in the absence of a sufficient food source and excyst when a food source becomes available. *Colpoda* cultures were derived from a cyst isolated from the rhizosphere of a bean plant grown in eastern Connecticut. Sequencing of the 18S gene using primers 384F (5′-YTBGATGGTAGTGTATTGGA) and 1147R (5′-GACGGTATCTRATCGTCTTT)[25] indicated that the isolate was *Colpoda* and its 18S was 98% identical with *Colpoda steinii*. Protist stocks were maintained in Page's saline solution in Nunc cell culture flasks with a 25 cm² culture area.

For culture propagation, 1 mL of encysted protists was added to 9 mL of sterile Page's saline and then *Escherichia coli* bacteria strain K12 were added at a final concentration of $7 \times 10^7$ cells mL⁻¹. To transfer protists from culture flasks for propagation or for use in experiments, cysts were scraped loose from the flask surface using a sterile plastic pipet tip, resuspended, and transferred to a new culture flask.

*Bacteria.* A variety of bacterial inputs were used during these experiments, depending upon the purpose of each experiment. Unfixed, unstained bacteria were used for protist culture propagation, because no fixative or stain was necessary. For bead transport experiments, the same unstained bacteria were used but these were fixed. For qualitative observations, fluorescent bacteria were used to facilitate direct observation in fixed form when the goal was to observe internal transport of bacteria and unfixed when the goal was to observe normal protist–bacteria interactions.

*E. coli* strain K12 were used to propagate cultures and induce protists to excyst during transport experiments. *E. coli* were grown to stationary phase at 30 °C for 24 h in lysogeny broth (LB) media, consisting of 10 g of tryptone, 5 g of yeast extract, and 10 g of sodium chloride in 1 L of deionized water. For transport assays, stationary-phase bacteria were fixed with gluteraldehyde (5%, final v/v), triple-washed, and resuspended in Page's saline. Then, $7 \times 10^7$ *E. coli* mL⁻¹ were combined with 1.0 $\mu$m Nile Red FluoSpheres carboxylate-modified polystyrene (PS) microspheres (Lot 991637, actual diameter of 1.1 ± 0.035 $\mu$m, Life Technologies, Grand Island, NY) at $3.5 \times 10^7$ beads mL⁻¹ in sterile Page's saline.

For imaging the interaction of bacteria with protists, green fluorescent protein (GFP)-expressing *P. fluorescens* (Pf5 and Pf0) was employed. *P. fluorescens* is a Gram-negative biocontrol strain that suppresses many plant pathogens and produces antibiotics. *P. fluorescens* were grown to stationary phase at 30 °C for 24 h in TY Media, consisting of 6 g of tryptone, 3 g of yeast extract, and 0.38 g of calcium chloride (anhydrous) in 1 L of deionized water, with kanamycin monosulfate at 25 $\mu$g mL⁻¹. When stationary-phase bacteria were fixed, gluteraldehyde was added at 5% (v/v), triple-washed, resuspended in Page's saline, diluted to an optical density of 0.01, and then added to microfluidic devices, as described below for the soil-patterned device. Images of bacteria uptake by protists were captured between 3 h and 10 days after *P. fluorescens* was combined with protists.

**Device Design and Fabrication.** An emulated soil pattern similar to that described by Deng et al.[26] was used to measure particle transport in a quiescent microstructured setting. The pattern emulates a pseudo-two-dimensional (2D) adaption of a three-dimensional (3D) packing of sandy loam-sized particles with a porosity of 0.47. Micromodels were comprised of three parallel microstructured channels connected at both ends by a wide, unstructured buffer region that was designed to isolate the microstructured regions from edge effects, as shown in Figure 1. The input well was punched at only one end, resulting in a dead-end volume, which prevented flow.

The microfluidic master was fabricated using the procedure detailed by Deng et al.,[27] with minor modifications. A 4 in. silicon wafer was spin-coated with SU-8 2025 to a height of 33.5 ± 1.5 $\mu$m. The coated wafer was patterned by exposure to
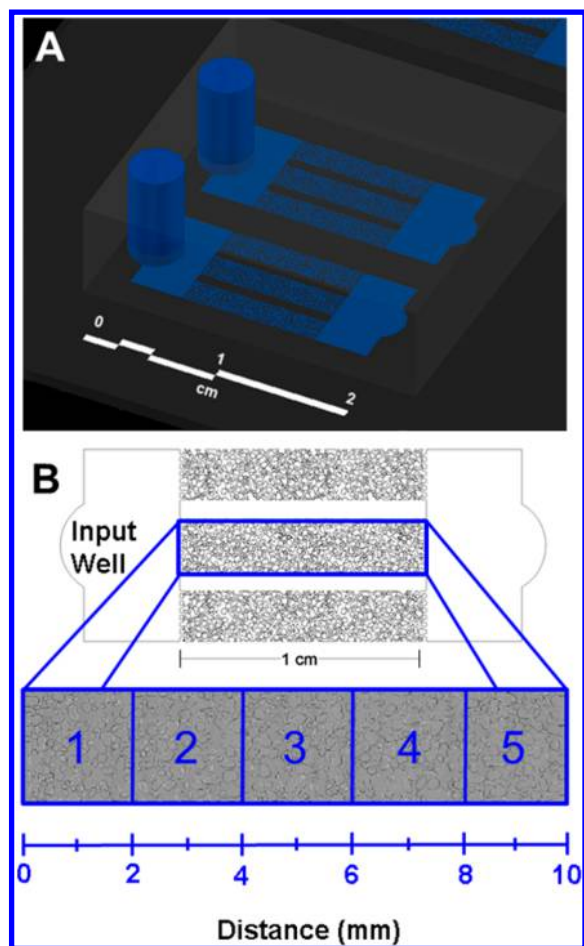
**Figure 1.** (A) Three-dimensional rendering of micromodels in AutoCAD. (B) Plan view of a single micromodel (scale bar below). The zoom is an example mosaic confocal micrograph of a single soil-patterned channel, showing zones as designated with distances from the start of the microstructured region given in the scale below.
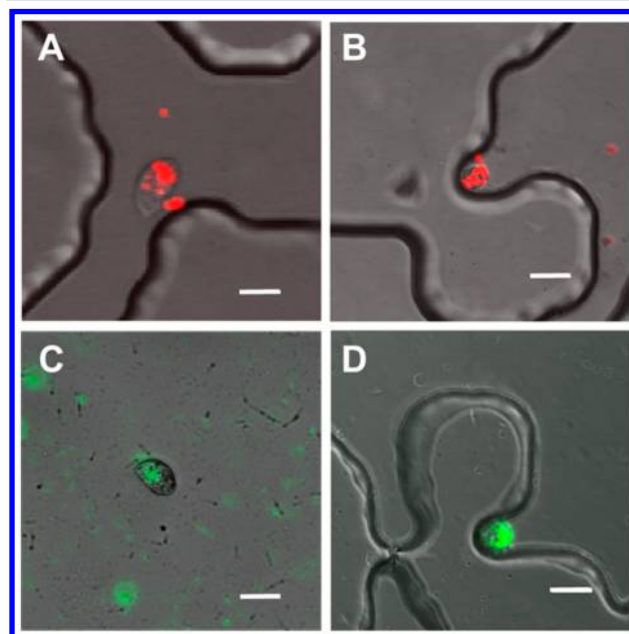


**Figure 2.** (A) Active *Colpoda* sp. carrying fluorescent red beads. (B) Encysted *Colpoda* sp. with fluorescent red beads. (C) Active *Colpoda* sp. in an unstructured microfluidic device, carrying unfixed GFP-expressing *P. fluorescens*. (D) Encysted *Colpoda* sp. in a soil-patterned microfluidic device carrying fixed GFP-expressing *P. fluorescens*. All scale bars are 20 $\mu$m.

ultraviolet light at 26.4 mW cm$^{-2}$ for 6.4 s with a chrome mask (Advance Reproductions, North Andover, MA). Replicate micromodels were cast from the master in polydimethylsiloxane (PDMS, Sylgard 184, Dow Corning, Midland, MI). A 4 mm biopsy punch was used to create the input wells. Punched castings were plasma-bonded to clean glass slides, featured side down, using the procedure also described by Deng et al.[27] The bonded devices were filled with sterile Page's saline solution and left undisturbed until trapped air dissipated, as shown in Figure S1 of the Supporting Information.

**Transport Experiments.** Protist-facilitated transport was determined by comparing the spatial distribution of fluorescent beads in replicate micromodels in the presence and absence of soil protists. Four replicate micromodels, each containing three parallel microstructured channels, were run simultaneously as shown in Figure S1 of the Supporting Information. Two replicates contained beads only, and two contained beads with protists.

Devices used for protist treatments were equilibrated with Page's saline, and then 30 $\mu$L was withdrawn from input wells (total well volume $\approx$ 88 $\mu$L) and replaced with 30 $\mu$L of 7 × 10$^3$ mL$^{-1}$ protist cysts suspended in Page's saline. The initial number of cysts added to each replicate was 8.1 × 10$^2$ and 5.0 × 10$^2$ cysts, respectively, corresponding to in-device concentrations of 9 × 10$^3$ and 5 × 10$^3$ cysts mL$^{-1}$, respectively. Next,

10 $\mu$L aliquots were carefully withdrawn from the top of each input well and replaced with 10 $\mu$L of the mixture of beads (3.5 × 10$^7$ mL$^{-1}$) and *E. coli* (7 × 10$^7$ mL$^{-1}$) in Page's saline. Input wells were covered with thin strips of PDMS to minimize evaporation. When not imaging, devices were stored in the dark at approximately 24 °C and 99% relative humidity.

**Imaging and Image Analysis.** Bacterial interactions with protists, including Figure 2C, were imaged using a Carl Zeiss AXIO-observer Z1 automated inverted microscope equipped with an AxioCam MRmRev.3 camera (Carl Zeiss, Inc., Germany). Bright-field and fluorescence (470 nm, 62 HE B/G/HR reflector, Carl Zeiss, Inc., Germany) images were captured using a 5× objective (Zeiss EC Plan-Neofluar).

For transport experiments, images were collected using a Nikon A1R confocal microscope system with an Eclipse Ti microscope and LU4 laser. Automated $x-y$ stage movement was used to capture full mosaic images of each microstructured channel. Nikon NIS Elements software was used to stitch the mosaics and apply shading correction. Images with beads were captured using a S Plan Fluor ELWD 20× DIC N1 objective, with resonance scanning capturing at 512 × 512 pixel resolution and the laser emitting at 595 nm. The image of an encysted *Colpoda* with *P. fluorescens* in Figure 2D was captured using the same objective but with galvano scanning at 2048 × 2048 pixel resolution and the laser emitting at 488 nm. Each channel was divided into five regions, as shown in Figure 1, and the number of beads and number of protists in each region were determined by direct counting after 1, 2, 3, 5, and 10 days. Beads inside actively swimming protists were excluded, but those inside encysted protists were counted. In the case of beads clustered together too tightly to count discretely, such as in egested food vacuoles, bead clusters were conservatively enumerated as 1 bead. Beads anywhere in the 33.5 $\mu$m channel

depth were visible at a single focal plane. The bead surface abundance per millimeter squared was computed based on the fluid-filled surface area of each region.

**Statistical Analysis and Modeling.** Statistical analysis was performed using Stata11. In the analysis, each of the three channels in replicate micromodels was treated as an independent observation (i.e., $n = 6$ per treatment). Diffusion of beads was simulated to confirm diffusive-type transport for a simplified micromodel geometry (see Figure S2 of the Supporting Information) using COMSOL Multiphysics 4.4. The simulation was constructed with a spatially uniform initial concentration of zero and a constant-concentration boundary condition at the input well interface (equal to $3.5 \times 10^7$ beads mL$^{-1}$ or $6.6 \times 10^{-12}$ mol m$^{-3}$, the calculated bulk concentration of beads added to the input well). All other edges were defined as no-flux boundaries. Per Norris and Sinko, who calculated and measured permeabilities of 1 $\mu$m carboxylate-modified PS beads with an initial concentration of $5.0 \times 10^7$ beads mL$^{-1}$, the initial bead concentration of $3.5 \times 10^7$ beads mL$^{-1}$ was assumed to be sufficiently dilute to model using Fickian diffusion.[28] The simulation was developed as a 2D, time-dependent model using the transport of diluted species module in COMSOL. To improve computational efficiency, the physical structure was not modeled explicitly; rather, the physical retardation ($R_p$) in the microstructured region was estimated as described previously[29]

$$D_{obs} = \frac{D_{mol}}{(R_p)(R_c)} = \frac{D_{mol}}{(\varepsilon^{-1/3})(R_c)}$$

where $D_{mol}$ is the molecular diffusion coefficient and $\varepsilon$ is the soil porosity. The carboxylated beads were assumed to behave as conservative tracers in the negatively charged PMDS and glass micromodels; therefore, chemical retardation, $R_c$, was assumed to be 1, similar to the assumption of no chemical retardation of a high-molecular-weight tracer in a micromodel by Singh and Olson.[30] Depletion of beads from the source well was found to be negligible (<1% after 10 days with a diffusivity of $1 \times 10^{-7}$ cm$^2$ s$^{-1}$), suggesting that the constant-concentration boundary condition assumption is reasonable.

## ■ RESULTS AND DISCUSSION

Three types of protist–particle interactions were observed. *Colpoda* sp. are voracious grazers and ingested both bacteria and beads, resulting in internal transport (Figure 2 and Video S4 of the Supporting Information). In addition, particles near protists were also observed being mixed or pushed along by the microcurrents created by the beating cilia of the protists (see Video S5 of the Supporting Information). This is in keeping with the need of protists to mix their immediate surroundings to graze efficiently, although the region of influence is small given the extremely low Reynolds numbers and probably does not extend beyond a few cell lengths. *P. fluorescens* bacteria were also observed adhering to the exterior surface of protists (see Video S6 of the Supporting Information). Although individual contributions were not determined, ingestion, fluid mixing, and attachment may each contribute to protist-facilitated transport of bacteria in real porous media.

These direct observations of protists interacting with bacteria lend to valuable insight. However, protist-facilitated transport of live, motile bacteria is a complex process, involving motility of both bacteria and protist, predator–prey interactions, and various parameters related to particle capture, residence time in

the protist, and digestion efficiency. Bacteria digestion rates by protists are highly variable by species and known to vary with prey abundance.[31] Given these inherent complexities, this initial investigation of protist-facilitated transport in emulated soil micromodels employed fluorescent beads as analogues for bacteria. The use of beads allowed for transport effects to be isolated from confounding effects of bacterial mobility, bacterial growth, and bacteria–protist trophic interactions, including capture and digestion efficiency.

Using beads as analogues for bacteria in feeding studies is well-established, and size has been determined to be a key selection criterion in ciliate grazing.[32] The beads used were selected because they are approximately the same size as typical protist prey. The carboxylate groups on the beads gave them a net negative surface charge similar to that of bacteria.[33] However, the $\zeta$ potential of similar beads has been reported by multiple sources to around $-60$ mV,[28,34] which is more negative than the typical range for bacteria.[33] Surface charges outside the typical range for bacteria have been shown to significantly reduce particle ingestion rates,[34] but ingestion was directly observed in this study. The density of the beads was about 1.05 g cm$^{-3}$, similar to bacteria density and close enough to the density of water to minimize density-driven transport effects. Bacteria were used in bead transport experiments because protists did not consistently excyst in the absence of a food source. Fixed bacteria were used because it has been shown that both free-swimming and attached bacteria can enhance mixing in microfluidic devices as a result of flagella stirring the surrounding fluid.[35,36] Protists were observed to excyst and reproduce in the presence of only fixed bacteria. Active bacteria might have resulted in greater numbers of active protists in the devices; therefore, the use of fixed bacteria likely resulted in a conservative estimate of transport.

During transport experiments, beads initially added to the input well were rapidly spread throughout the microstructured regions of replicate channels in treatments with protists but reached the microstructured regions much more slowly without protists present. A representative subsection of region 1 for treatments with and without protists is shown after 1, 2, 3, 5, and 10 days (Figure 3). In the with-protists treatment, bead abundance increased rapidly, with about 30 beads visible in that subsection after 2 days. The abundance of beads continued to increase to about 35 beads after 3 days, 43 beads after 5 days, and then dropped slightly to 36 beads after 10 days. In contrast, the abundance of beads in the corresponding subsection in the without-protists treatment was still zero after 2 days; 2 beads were visible after 3 days; 11 beads were visible after 5 days; and after 10 days, approximately 14 beads were visible. For this particular subsection, bead abundance in the with-protists treatment was double the without-protists abundance in one-fifth the time. The relative enhancement in bead transport rates between the two treatments varied widely with position and time, suggesting that beads may have been transported by different mechanisms in the two treatments.

Patterns in bead surface abundance or the number of beads counted in a given region divided by the fluid-filled area in that region were analyzed across treatments, replicates, channels, and regions. One striking feature is the dramatically increased surface abundance in region 1 compared to the other regions (Figure 4). The fact that surface abundance is highest in region 1 is not surprising, given that it is closest to the input well where beads were initially added. However, trends among the other regions were less predictable. Excluding region 1, an
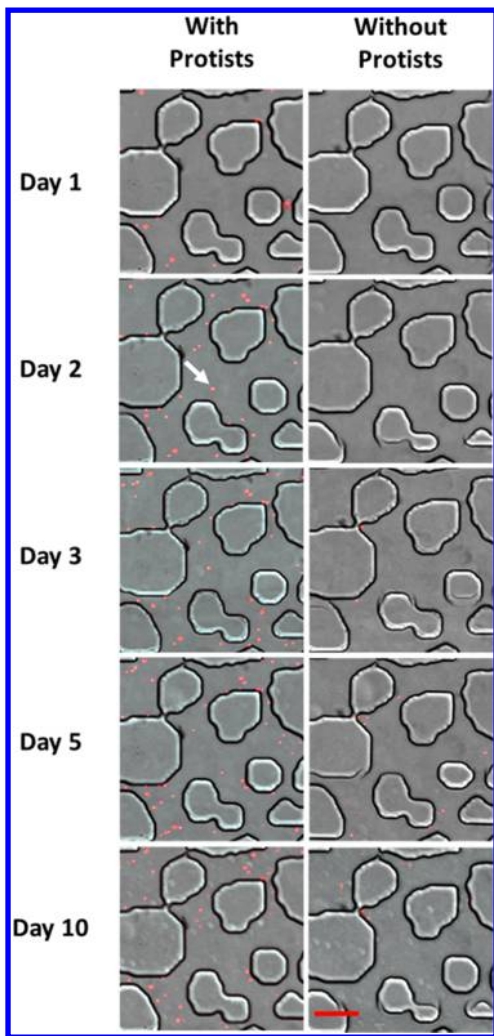
**Figure 3.** Beads in a small portion of region 1 with treatment and time. The arrow indicates a single fluorescent bead. The scale bar is 100 $\mu$m.

analysis of variation (ANOVA) across the remaining regions (i.e., 2, 3, 4, and 5) was significant only at the later time points ($F(3,20) = 4.94$, with $p = 0.010$ at 5 days, and $F(3,20) = 5.96$, with $p = 0.005$ at 10 days). At 1, 2, and 3 days, the ANOVA of bead surface abundance with protists across regions 2, 3, 4, and 5 was not significantly different from a uniform distribution, despite the reproducibility in measured bead abundance. In contrast, in a diffusion context with a zero initial concentration throughout the micromodel volume and a large concentration at one boundary, one might expect significant spatial variation at all points in time, including the early time periods.

In treatments with protists, the trend in bead surface abundance with time was similar between regions. In each case, bead abundance rapidly increased through day 3 and then increased more slowly, stayed flat, or decreased slightly between 5 and 10 days (Figure 5). Although the magnitude of surface abundance was much higher in region 1, the shapes of the abundance versus time curves were qualitatively similar across regions, with deposition rates decreasing with time in every region (Figure 5B). Average deposition rates in beads per day indicate that more than 200 beads were deposited in the first day in the first region and that deposition rates were a strong function of time but not of position outside the first region.

Protists influenced the spatial and temporal distribution of beads in these micromodels. The influence of protists was likely impacted by the number, activity, and spatial distribution of protists as well as by the proportion of active versus encysted protists. Protist abundance in microchannels was estimated by enumerating animate and encysted protists in tiled micrographs whenever beads were enumerated. The variability in the resulting protist abundance data was high, perhaps because the imaging frequency was low compared to the frequency and range of fluctuations in protist distribution within the microstructured channels. Although it was anticipated that, like beads, the abundance of protists would be higher in the region nearest the input well, in fact, there was no statistically significant trend in protist abundance with position. Protists
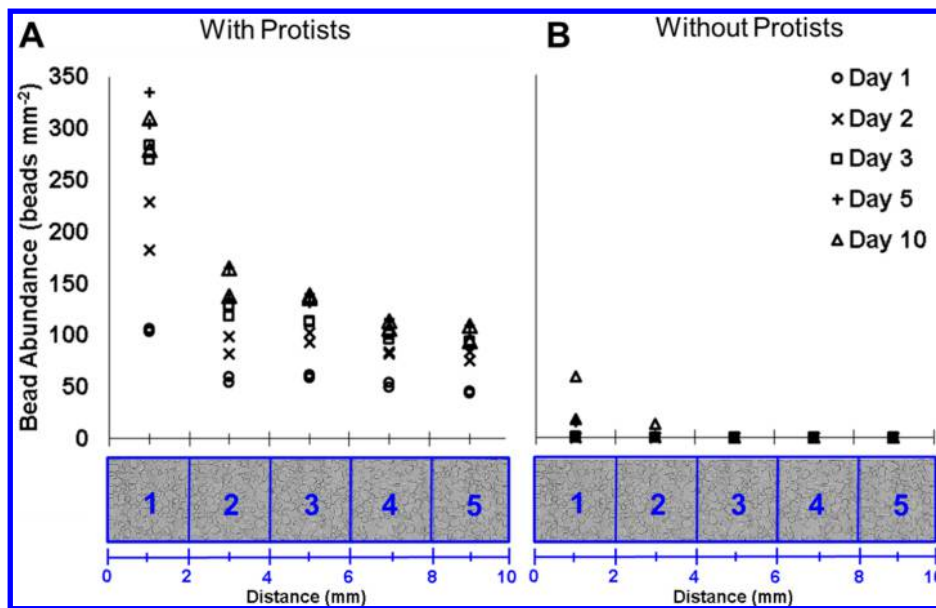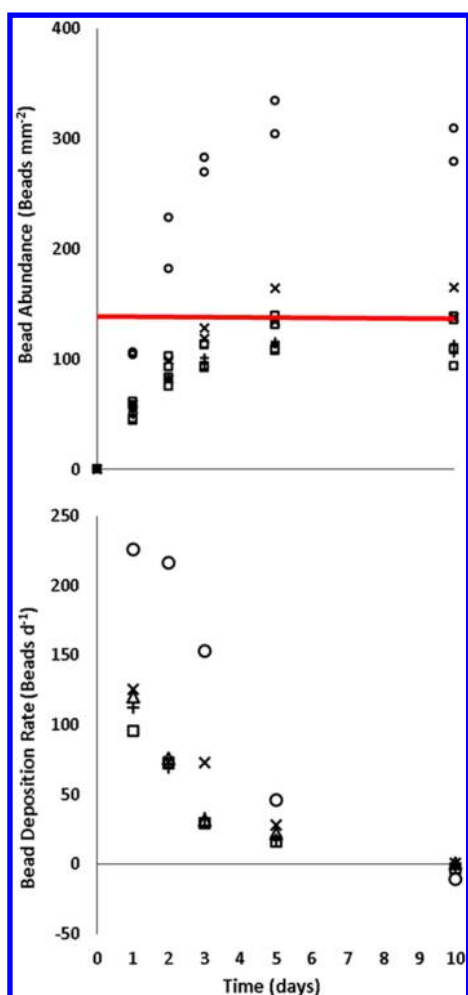


**Figure 4.** Spatial distribution of fluorescent beads in the microstructured channels of replicate micromodels (A) with *Colpoda* sp. present and (B) without protists present. The average surface abundances among all three channels are shown separately for replicate micromodels. Data markers reflect elapsed time at imaging: (◯) 1 day, (×) 2 days, (☐) 3 days, (+) 5 days, and (△) 10 days.

**Figure 5.** (A) Bead surface abundance in the with-protists treatment versus time at different positions along the microstructured channels. The average surface abundance among all three channels is shown separately for duplicate micromodels. The horizontal line at 140 beads mm$^{-2}$ reflects the surface abundance if beads are evenly distributed throughout the micromodel volume. (B) Average deposition rate of beads with protists over time across all channels and replicates ($n = 6$). Data markers and line types indicate the region within the microstructured channel: (O) region 1, ($\times$) region 2, ($\triangle$) region 3, (+) region 4, and ($\square$) region 5.

were frequently observed to change direction and return to the input well after only partially traversing a channel, and instantaneous protist abundance in a given region changed more frequently than images were collected. More precise determinations of protist abundance and encystment rates with position and time could provide insight into the mechanism of protist-facilitated bead transport in porous media.

While protist abundance was variable, there was a general decreasing trend in the number of protists (active and encysted) with time (Figure 6). Abundances after 5 and 10 days were significantly different from abundances after 1, 2, or 3 days [paired $t(5) > 3.89$, with $p < 0.012$, two tailed]. Protist abundance was not significantly different between 1 and 2 days, between 2 and 3 days, or between 5 and 10 days. In addition to the change in total protist abundance, deposition rates were probably also influenced by the declining proportion of active protists. *Colpoda* sp. re-encyst as the food supply declines. No additional bacteria were added during the experiment after the
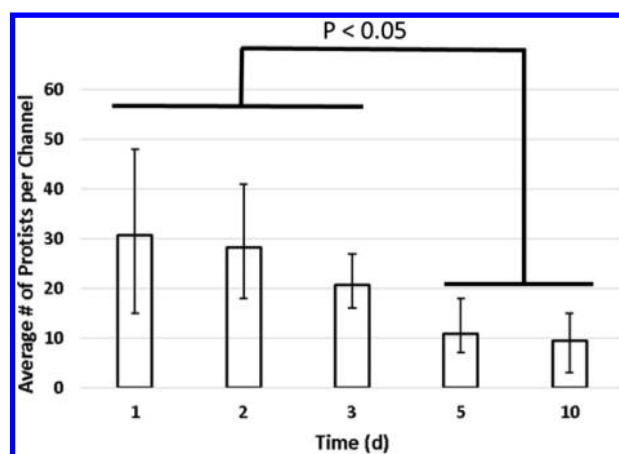


**Figure 6.** Average number of protists in all channels ($n = 6$) with time. Bars reflect the range of average abundances in each channel.

initial loading, and bacterial prey were likely becoming depleted by 5 or 10 days.

The diffusivity of the 1.1 $\mu$m PS beads was estimated to be 4 $\times$ 10$^{-9}$ cm$^2$ s$^{-1}$ using the Stokes–Einstein equation.[37] Schmitz et al. also used this method to estimate the diffusivity of unmodified 0.109 $\mu$m PS beads in aqueous solutions and validated the results with experimental measurements.[38] As described previously, a finite element simulation in the soil micromodel geometry was performed using COMSOL Multiphysics. Iterative parameter sweeps and minimization of error between measured and simulated bead surface abundance suggested a bead diffusivity of approximately 6 $\times$ 10$^{-8}$ cm$^2$ s$^{-1}$ (see Figure S3 of the Supporting Information) in the without-protists treatment. Although the parameter value is higher than the estimated diffusivity calculated using the Stokes–Einstein equation, the bead abundance counts over time for the without-protists treatment seem to exhibit a trend consistent with a Fickian diffusion mechanism and the trend is clearly different from the with-protists case. Given that a higher than expected diffusive mobility was not observed in studies investigating PS bead diffusion in bulk liquids,[28,38] the higher diffusive mobility of beads observed here may have been the result of surface interactions between the beads and the PDMS walls in the microdevice, including electrostatic interactions, or the result of concentration-dependent diffusivity. However, because these factors would also have been present in the with-protist treatments, the difference in bead abundance between the two treatments still points to a marked protist-facilitated transport effect.

The magnitude of bead surface abundance suggests that interactions between beads and protists not only leads to a facilitated transport effect but may also result in a super-abundance of beads in microstructured settings. A uniform distribution of beads throughout the micromodel would lead to a surface abundance in the channel of approximately 140 beads mm$^{-2}$. However, after 10 days with protists, measured surface abundance in region 1 was 300 beads mm$^{-2}$ or an enrichment factor of approximately 2. The mechanism responsible for this superabundance of beads is not known but may arise from interacting physical and biological factors. For example, it is likely that most beads in the microstructured channels had been egested in packages of multiple beads, which are larger than the optimal size for protist grazing, reducing the likelihood of re-ingestion. The larger size of these packages may also have

enhanced their settling rate, and the biopolymers holding the packages together may have promoted surface attachment, thereby preventing subsequent transport. Given the spatial arrangement and high surface area of the channel, the net effect may be a bias of inward over outward transport.

Eventually, protist-facilitated transport and accumulation of particles in microstructured settings may be successfully modeled using an agent-based approach with measured parameter distributions, including swimming speeds, run lengths, turning angles, bead capture efficiency, particle residence time in protists, and encystment rates. Further extensions to include living, motile, variably digested bacterial populations and to account for inhibition in unsaturated porous media could help predict the utility and magnitude of protist-facilitated transport effects at the field scale.

Here, the effect of protists on the rate and extent of transport of polystyrene microspheres was measured in an emulated soil micromodel. These results, together with literature reports on the ability of bacteria to survive and thrive after egestion, suggest that protist-facilitated transport could be used to enhance various ecosystem services of soil bacteria. Protist-facilitated transport could be used to enhance sustainable agricultural productivity via targeted delivery of biocontrol bacteria or encapsulated agrochemicals directly to the roots of plants. Similarly, protists could be used as a non-invasive means of conveyance for key bacterial strains or co-metabolites to improve the performance of *in situ* bioremediation. Understanding and optimizing this phenomena for use in the field will require extensive further research that is enabled by the experimental techniques described here.

## ASSOCIATED CONTENT

### Ⓢ Supporting Information

Schematic of the experimental setup and photograph of micromodels bonded to a glass slide as used for the experiments (Figure S1), simplified physical geometry used for the diffusion simulation (Figure S2), COMSOL-modeled diffusion together with the measured data for beads in the without-protists treatment (Figure S3), and three mechanisms of transport observed (Videos S4−S6). This material is available free of charge via the Internet at http://pubs.acs.org.

## AUTHOR INFORMATION

### Corresponding Author

*Telephone: 860-486-3136. Fax: 860-486-2959. E-mail: leslieshor@gmail.com.

### Notes

The authors declare no competing financial interest.

## ACKNOWLEDGMENTS

## REFERENCES

(1) Kinner, N. E.; Harvey, R. W.; Shay, D. M.; Metge, D. W.; Warren, A. Field evidence for a protistan role in an organically-contaminated aquifer. *Environ. Sci. Technol.* **2002**, *36* (20), 4312−4318.

(2) Druhan, J. L.; Bill, M.; Lim, H.; Wu, C.; Conrad, M. E.; Williams, K. H.; DePaolo, D. J.; Brodie, E. L. A large column analog experiment of stable isotope variations during reactive transport: II. Carbon mass balance, microbial community structure and predation. *Geochim. Cosmochim. Acta* **2014**, *124*, 394−409.

(3) Tso, S. F.; Taghon, G. L. Protozoan grazing increases mineralization of naphthalene in marine sediment. *Microb. Ecol.* **2006**, *51*, 460−469.

(4) Cunningham, J. J.; Kinner, N. E.; Lewis, M. Protistan predation affects trichloroethene biodegradation in a bedrock aquifer. *Appl. Environ. Microbiol.* **2009**, *75* (24), 7588−7593.

(5) Mittal, M.; Rockne, K. J. Dynamic models of multi-trophic interactions in microbial food webs. *J. Environ. Sci. Health, Part A: Toxic/Hazard. Subst. Environ. Eng.* **2012**, *47* (10), 1391−1406.

(6) Ranjard, L.; Richaume, A. S. Quantitative and qualitative microscale distribution of bacteria in soil. *Res. Microbiol.* **2001**, *152* (8), 707−716.

(7) Or, D.; Smets, B. F.; Wraith, J. M.; Dechesne, A.; Friedman, S. P. Physical constraints affecting bacterial habitats and activity in unsaturated porous media—A review. *Adv. Water Resour.* **2007**, *30* (6−7), 1505−1527.

(8) Song, X.; Seagren, E. A. In situ bioremediation in heterogeneous porous media: Dispersion-limited scenario. *Environ. Sci. Technol.* **2008**, *42* (16), 6131−6140.

(9) Wick, L. Y.; Mattle, P. A.; Wattiau, P.; Harms, H. Electrokinetic transport of PAH-degrading bacteria in model aquifers and soil. *Environ. Sci. Technol.* **2004**, *38* (17), 4596−4602.

(10) Kohlmeier, S.; Smits, T. H.; Ford, R. M.; Keel, C.; Harms, H.; Wick, L. Y. Taking the fungal highway: Mobilization of pollutant-degrading bacteria by fungi. *Environ. Sci. Technol.* **2005**, *39* (12), 4640−4646.

(11) Singer, A.; Jury, W.; Luepromchai, E.; Yahng, C.-S.; Crowley, D. Contribution of earthworms to PCB bioremediation. *Soil Biol. Biochem.* **2001**, *33* (6), 765−776.

(12) Armitage, J. P.; Pitta, T. P.; Vigeant, M. A.-S.; Packer, H. L.; Ford, R. M. Transformations in flagellar structure of *Rhodobacter sphaeroides* and possible relationship to changes in swimming speed. *J. Bacteriol.* **1999**, *181* (16), 4825−4833.

(13) Madsen, E. L.; Alexander, M. Transport of *Rhizobium* and *Pseudomonas* through soil. *Soil Sci. Soc. Am. J.* **1982**, *46* (3), 557−560.

(14) Eisenmann, H.; Harms, H.; Meckenstock, R.; Meyer, E. I.; Zehnder, A. J. Grazing of a *Tetrahymena* sp. on adhered bacteria in percolated columns monitored by in situ hybridization with fluorescent oligonucleotide probes. *Appl. Environ. Microbiol.* **1998**, *64* (4), 1264−1269.

(15) Korber, D. R.; Lawrence, J. R.; Sutton, B.; Caldwell, D. E. Effect of laminar flow velocity on the kinetics of surface recolonization by Mot⁺ and Mot⁻ *Pseudomonas fluorescens*. *Microb. Ecol.* **1989**, *18* (1), 1−19.

(16) Wang, W.; Shor, L. M.; LeBoeuF, E. J.; Wikswo, J. P.; Taghon, G. L.; Kosson, D. S. Protozoa migration in bent microfluidic channels. *Appl. Environ. Microbiol.* **2008**, *74* (6), 1945−1949.

(17) Boenigk, J.; Matz, C.; Jürgens, K.; Arndt, H. The influence of preculture conditions and food quality on the ingestion and digestion process of three species of heterotrophic nanoflagellates. *Microb. Ecol.* **2001**, *42* (2), 168−176.

(18) First, M. R.; Park, N. Y.; Berrang, M. E.; Meinersmann, R. J.; Bernhard, J. M.; Gast, R. J.; Hollibaugh, J. T. Ciliate ingestion and digestion: Flow cytometric measurements and regrowth of a digestion-resistant *Campylobacter jejuni*. *J. Eukaryotic Microbiol.* **2012**, *59* (1), 12−19.

(19) Brock, D. A.; Douglas, T. E.; Queller, D. C.; Strassmann, J. E. Primitive agriculture in a social amoeba. *Nature* **2011**, *469* (7330), 393−396.

(20) Young, I. M.; Crawford, J. W. Interactions and self-organization in the soil-microbe complex. *Science* **2004**, *304* (5677), 1634−1637.

(21) Long, T.; Ford, R. M. Enhanced transverse migration of bacteria by chemotaxis in a porous T-sensor. *Environ. Sci. Technol.* **2009**, *43* (5), 1546−1552.

(22) Wang, W.; Shor, L. M.; LeBoeuf, E. J.; Wikswo, J. P.; Kosson, D. S. Mobility of protozoa through narrow channels. *Appl. Environ. Microbiol.* **2005**, *71* (8), 4628−4637.

(23) Cho, H.; Jönsson, H.; Campbell, K.; Melke, P.; Williams, J. W.; Jedynak, B.; Stevens, A. M.; Groisman, A.; Levchenko, A. Self-organization in high-density bacterial colonies: Efficient crowd control. *PLoS Biol.* **2007**, *5* (11), No. e302.

(24) Kim, H. J.; Boedicker, J. Q.; Choi, J. W.; Ismagilov, R. F. Defined spatial structure stabilizes a synthetic multispecies bacterial community. *Proc. Natl. Acad. Sci. U. S. A.* **2008**, *105* (47), 18188−18193.

(25) Dopheide, A.; Lear, G.; Stott, R.; Lewis, G. Molecular characterization of ciliate diversity in stream biofilms. *Appl. Environ. Microbiol.* **2008**, *74* (6), 1740−1747.

(26) Deng, J.; Orner, E. P.; Chau, J. F.; Anderson, E. M.; Kadilak, A. L.; Rubinstein, R. L.; Bouchillon, G. M.; Goodwin, R. L.; Gage, D. J.; Shor, L. Synergistic effects of soil microstructure and bacterial EPS on drying rate in emulated soil micromodels. *Soil Biol. Biochem.* **2015**, DOI: 10.1016/j.soilbio.2014.12.006.

(27) Deng, J.; Dhummakupt, A.; Samson, P. C.; Wikswo, J. P.; Shor, L. M. Dynamic dosing assay relating real-time respiration responses of *Staphylococcus aureus* biofilms to changing micro-chemical conditions. *Anal. Chem.* **2013**, *85* (11), 5411−5419.

(28) Norris, D. A.; Sinko, P. J. Effect of size, surface charge, and hydrophobicity on the translocation of polystyrene microspheres through gastrointestinal mucin. *J. Appl. Polym. Sci.* **1997**, *63* (11), 1481−1492.

(29) Shor, L. M.; Rockne, K. J.; Taghon, G. L.; Young, L.; Kosson, D. S. Desorption kinetics for field-aged polycyclic aromatic hydrocarbons from sediments. *Environ. Sci. Technol.* **2003**, *37* (8), 1535−1544.

(30) Singh, R.; Olson, M. S. Transverse mixing enhancement due to bacterial random motility in porous microfluidic devices. *Environ. Sci. Technol.* **2011**, *45* (20), 8780−8787.

(31) Tuorto, S.; Taghon, G. Rates of benthic bacterivory of marine ciliates as a function of prey concentration. *J. Environ. Mar. Biol. Ecol.* **2014**, *460*, 129−134.

(32) Fenchel, T. Suspension feeding in ciliated protozoa: Functional response and particle size selection. *Microb. Ecol.* **1980**, *6* (1), 1−11.

(33) Gannon, J.; Manilal, V.; Alexander, M. Relationship between cell surface properties and transport of bacteria through soil. *Appl. Environ. Microbiol.* **1991**, *57* (1), 190−193.

(34) Hammer, A.; Grüttner, C.; Schumann, R. The effect of electrostatic charge of food particles on capture efficiency by *Oxyrrhis marina* Dujardin (Dinoflagellate). *Protist* **1999**, *150* (4), 375−382.

(35) Kim, M. J.; Breuer, K. S. Use of bacterial carpets to enhance mixing in microfluidic systems. *J. Fluids Eng.* **2007**, *129* (3), 319.

(36) Kim, M. J.; Breuer, K. S. Controlled mixing in microfluidic systems using bacterial chemotaxis. *Anal. Chem.* **2007**, *79* (3), 955−959.

(37) Edward, J. T. Molecular volumes and the Stokes−Einstein equation. *J. Chem. Educ.* **1970**, *47* (4), 261.

(38) Schmitz, K. S.; Lu, M.; Gauntt, J. Influence of ionic strength on the diffusion of polystyrene latex spheres, bovine serum albumin, and polynucleosomes. *J. Chem. Phys.* **1983**, *78* (8), 5059−5066.